LAWRENCE
LIVERMORE
NATIONAL
LABORATORY

LLNL-CONF-434276

Dependence of Transport on the Safety Factor Profile in DIII-D Steady-state Scenarios

C. Holcomb, J. Ferron, A. White, T. Luce, J. DeBoo, T. Rhodes, L. Schmitz, F. Turco

June 7, 2010

European Physical Society 37th Conference on Plasma Physics
Dublin, Ireland
June 21, 2010 through June 25, 2010

Disclaimer

Dependence of Transport on the Safety Factor Profile in DIII-D Steady-state Scenarios

C.T. Holcomb[1], J.R. Ferron[2], A.E. White[3], T.C. Luce[2], J.C. DeBoo[2], T.L. Rhodes[4], L. Schmitz[4], F. Turco[5]

[1]*Lawrence Livermore National Laboratory, Livermore, California, 94551, USA*
[2]*General Atomics, PO Box 85608, San Diego, California 92186, USA*
[3]*Oak Ridge Institute for Science & Education, PO Box 117, Oak Ridge, Tennessee, 37831, USA*
[4]*University of California, Los Angeles, California 90095, USA*
[5]*Oak Ridge Associated Universities, PO Box 117, Oak Ridge, Tennessee 37831, USA*

I. Introduction

Recent steady-state scenario experiments on DIII-D examined the complex and recursive relationship between the choice of target safety factor (q) profile and the resulting transport, density and temperature profiles, and bootstrap current density at high noninductive current fraction [1]. This paper focuses on the transport and profile variation in a set of nine discharges in which the edge and minimum q (q_{95} and q_{min}) were scanned. These discharges were all ramped up to and held fixed at $\beta_N = \beta_T(\%)/\left[I_p(\mathrm{MA})/a(\mathrm{m})B_T(\mathrm{T})\right]$ = 2.8 using neutral beams under feedback control. The toroidal field B_T = 2.0 Tesla, and the discharge shape was fixed to a slightly unbalanced double-null divertor, so q_{95} was varied by adjusting the plasma current I_P. q_{min} was varied by adjusting the early-time power and H-mode transition time. Electron cyclotron current drive power was driven in a broad region centered at mid-radius to maintain broad, tearing mode-stable current profiles. The formation of deeply reversed magnetic shear and internal transport barriers was explicitly avoided in these experiments. No attempt was made to control the radius of q_{min}.

The q-profiles were determined using the EFIT equilibrium reconstruction code [2] with the following constraints: edge magnetic sensors, Motional Stark Effect internal field pitch angle measurements [3], a pressure profile determined by measurements of density and temperature and a Monte Carlo calculation of the fast ion pressure (NUBEAM code [4]), and a pedestal current density set by the Sauter bootstrap current model [5] contained within the ONETWO transport code [6]. For each discharge, a period of 200 to 1200 ms was identified with $\beta_N \approx 2.8$ and no large tearing modes present. All profiles shown here are the mean profile during this time period, and the error bars denote plus and minus one standard deviation. Stated values of q_{95} and q_{min} are mean values in these periods. Most of this paper focuses on a comparison of the four discharges at the extremes of the q_{95} and q_{min} scans, henceforth referred to as "the scan endpoints". The same color-coding is used for these throughout: red is q_{95}=4.5, q_{min}=1.7, black is q_{95}=6.8, q_{min}=1.9, blue is q_{95}=4.5, q_{min}=1, and green is q_{95}=6.8, q_{min}=1. These q, density and temperature profiles are shown in Figures 1 and 2.

II. Density and Temperature Profile Dependence on q_{95} and q_{min} at fixed β_N=2.8

Systematic differences with q_{95} and q_{min} greater than the error bars are observed in electron density (n_e) and temperature (T_e), and ion density (n_i) and temperature (T_i). The core

n_e, T_e, n_i and T_i all decrease with q_{95} in agreement with global energy confinement scaling with I_P. At any q_{95}, T_e and T_i increase with q_{min}. Increasing q_{min} broadens the T_e profile by increasing its gradient over the outer half-radius and decreasing it inside. The H-mode pedestal density decrease with q_{min} does not hold in general in the full 9-discharge dataset.

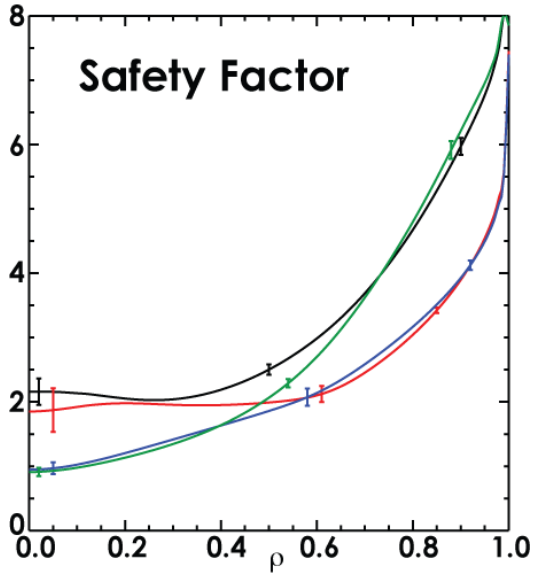

Figure 1 Mean q-profiles produced in a scan of q_{95} and q_{min} at fixed β_N=2.8 (4 scan endpoints shown)

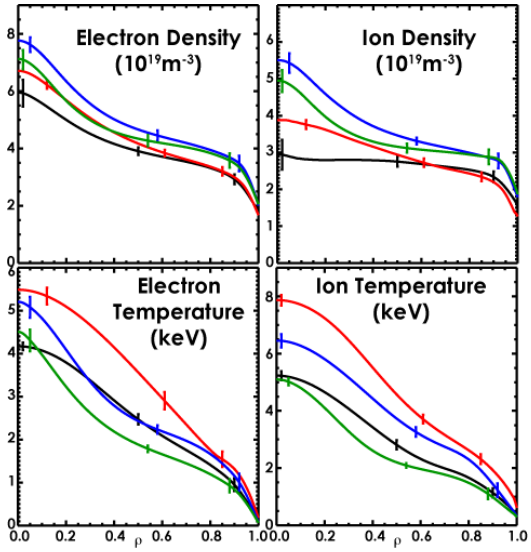

Figure 2 Mean density and temperature profiles associated with the Fig. 1 q-profiles (same color coding) show systematic differences with q

III. Thermal Diffusivity and Power Balance Dependence on q_{95} and q_{min} at fixed β_N=2.8

Thermal diffusivity (χ) profiles were calculated using ONETWO with the experimental profiles of current density, density, temperature, rotation, and radiated power as input, as well as the injected neutral beam and electron cyclotron heating power. Figures 3 and 4 show χ_e and χ_i for the scan endpoints. The maximum value of χ_i near ρ=0.6-0.7 increases with q_{95}, while χ_e is less sensitive to q_{95}, especially at low q_{min}. The insets in Figures 3 and 4 use the full 9-discharge data set and show variation of the mean $\chi(\rho=0.7)$ with q_{95} and q_{min}. χ_e generally decreases with q_{min}, while χ_i stays the same or increases with q_{min}.

Figure 5 shows the power balance of the scan endpoints. The bars indicate mean power to (positive) or from (negative) ions (red) and electrons (blue) during the analysis time period. The categories are neutral beam injection (NBI), ion to electron exchange (i→e), conduction plus convection (Cd+Cv), electron cyclotron heating (ECH), and radiation (Rad). Power to the electrons from Ohmic heating and charge exchange and recombination are approximately equal in these discharges and small on these plots, so they are not shown. Figure 5 indicates that at low q_{min}, electrons are the dominant loss channel, but as q_{min} increases the electron transport improves and the ions become the dominant loss channel by a small amount. The ion to electron energy exchange and T_i/T_e decrease with q_{95} because T_e decreases less with q_{95} than T_i does. In the full 9-shot dataset, T_i/T_e from ρ~0 to ~0.7 is minimized at intermediate values of q_{min}~1.4-1.6.

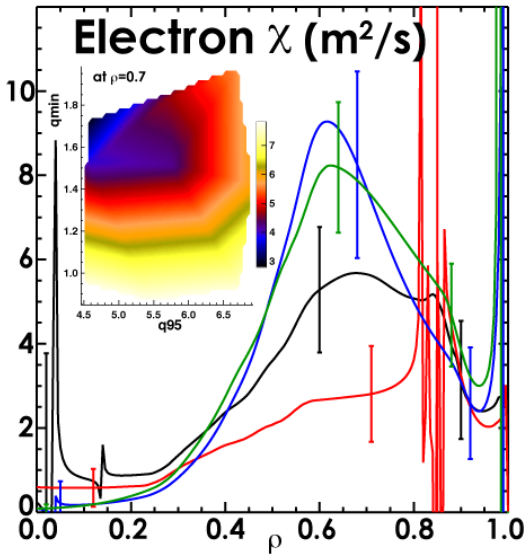

Figure 3 Mean electron thermal diffusivity profiles (Fig. 1 color coding) and contours of $\chi_e(\rho=0.7)$ vs. q_{95} and q_{min} using the full dataset (inset)

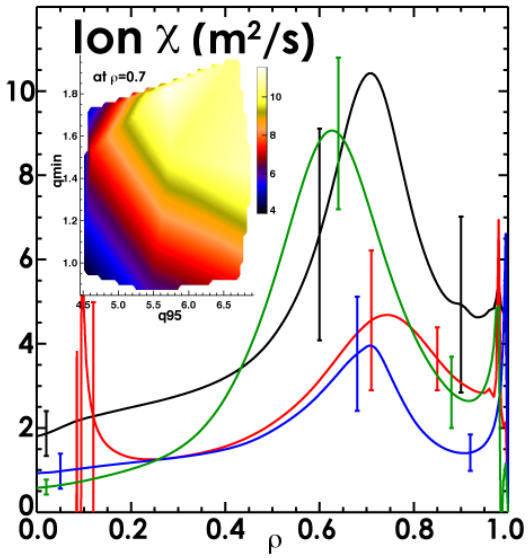

Figure 4 Mean ion thermal diffusivity profiles (Fig. 1 color coding) and contours of $\chi_i(\rho=0.7)$ vs. q_{95} and q_{min} using the full dataset (inset)

IV. Comparison to Turbulence Measurements and Drift Wave Stability Analysis

In the absence of large-scale MHD, anomalous transport is usually attributed to drift-wave turbulence [7], typically low poloidal wave number (k_θ) ion temperature gradient modes, intermediate-k_θ trapped electron modes, and high-k_θ electron temperature gradient modes. In this view, the q-scaling of (*i*) turbulence measurements, (*ii*) calculations of drift wave growth rates, and (*iii*) χ's determined by power balance should all be consistent.

Figure 6 shows Far Infrared Scattering (FIR) [8] measurements of line-averaged low-k_θ density fluctuation amplitudes versus time for the scan endpoints. Analysis time periods begin after t=3 s. Turbulence increases with q_{95} and even more strongly with q_{min}, which is consistent with the calculated worsening of ion transport with q_{95} and q_{min}. Intermediate and high-k_θ FIR measurements were below the noise levels so any differences are not discernible.

Drift wave linear stability analysis of the full dataset was performed using the trapped-gyro Landau fluid (TGLF) model [9] at multiple radii. The TGLF code was given measured profiles as inputs to calculate the growth rate (γ) and frequency of the most unstable mode at each k_θ. Figure 7 shows low- and high-k_θ results at ρ=0.6 for the scan endpoints. Flat lines in the low-k_θ γ-plot are the local ExB shear quench rates [10]. If this exceeds γ the mode may be stabilized. Positive/(negative) frequency is typically interpreted as an electron/(ion) mode.

The results are not universally consistent with the observed transport scalings. While ion and electron transport increases with q_{95}, γ's at all k_θ decrease with q_{95}. Some high q_{95} cases with large χ_i nonetheless have low-k_θ γ's less than the quench rate (e.g. the green curve in Figure 7). These results also contradict the low-k_θ turbulence measurements. The low-k_θ γ's do increase with q_{min}, in agreement with the observed increase of χ_i with q_{min}, but the high-k_θ γ's increase with q_{min}, contrary to the observed decrease in χ_e with q_{min}. γ/k_θ^2 estimates the diffusivity due to these modes, and in all discharges it suggests intermediate and high-k_θ electron modes are irrelevant for transport compared to low-k_θ ion modes. This is at odds

with the power balance showing electrons contributing significantly to total transport losses.

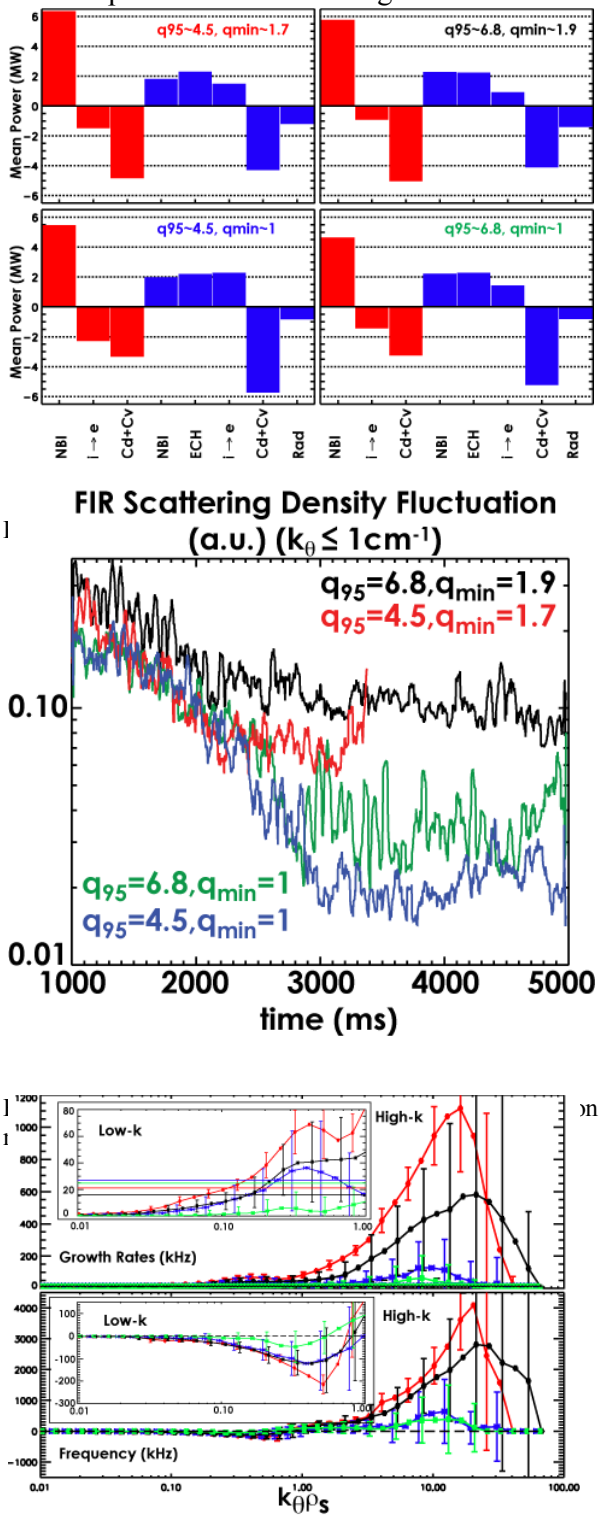

Figure 7 Drift wave growth rate and frequency of the scan endpoints from TGLF linear stability analysis at ρ=0.6; same color coding as Fig. 1 (ρ_s≡ion gyroradius)

V. Discussion and Conclusions

The unexpected decrease in electron transport and broadening of T_e with q_{min} is perhaps beneficial for scenarios that seek to maximize bootstrap current with elevated q_{min}. A caveat in this analysis is that there is evidence for anomalous transport of fast ions increasing with q_{min}, but the fast ion transport was taken to be neoclassical. If this loss was underestimated in the higher q_{min} discharges, then the ion transport may not increase as much with q_{min}, and the electron transport may decrease more with q_{min} then this analysis indicates. The inconsistent q-dependence of the linear stability analysis results and the observed transport shows the need for nonlinear TGLF analysis to account for possible mode coupling, further experimental tests of transport in high β_N scenarios, and further model validation.

This work was supported by the US Department of Energy under DE-AC52-07NA27344(LLNL) and DE-FC02-04ER54698.

References

[1] J.R. Ferron *et al.*, to be submitted to Nucl. Fusion
[2] L.L. Lao *et al.*, Nucl. Fusion **30**, 1035 (1990).
[3] B.W. Rice *et al.*, Phys. Rev. Lett. **79**, 2694 (1997).
[4] A. Pankin *et al.*, Comput. Phys. Commun. **159**, 157 (2004).
[5] O. Sauter *et al.*, Phys. Plasmas **6**, 2834 (1999).
[6] H.E. St. John *et al.*, *Proceedings of the 15th International Conference on Plasma Physics and Controlled Nuclear Fusion Research*, Seville, Spain, 1994 (IAEA, Vienna, 1995), Vol. 3, p. 603.
[7] E.J. Doyle *et al.*, Nucl. Fusion **47**, S18-S127 (2007).
[8] C.L. Rettig *et al.*, Rev. Sci. Instrum. **61**, 10 (1990).
[9] G.M. Staebler *et al.*, Phys. Plasmas, **14**, 055909 (2007).
[10] J.E. Kinsey *et al.*, Phys. Plasmas, **15**, 055908 (2008).